Emergent room temperature polar phase in $CaTiO_3$ nanoparticles and single crystals

Cite as: APL Mater. 7, 011103 (2019); doi: 10.1063/1.5078706
Submitted: 28 October 2018 • Accepted: 19 December 2018 •
Published Online: 22 January 2019

Mariola O. Ramirez,[1,a] Tom T. A. Lummen,[2] Irene Carrasco,[3,b] Eftihia Barnes,[2] Ulrich Aschauer,[4,c] Dagmara Stefanska,[5] Arnab Sen Gupta,[2] Carmen de las Heras,[1] Hirofumi Akamatsu,[2] Martin Holt,[6] Pablo Molina,[1] Andrew Barnes,[2] Ryan C. Haislmaier,[2] Przemyslaw J. Deren,[5] Carlos Prieto,[7] Luisa E. Bausá,[1] Nicola A. Spaldin,[8] and Venkatraman Gopalan[2,a]

AFFILIATIONS

[1]Departamento Física de Materiales, Instituto Nicolás Cabrera and Condensed Matter Physics Center (IFIMAC), Universidad Autónoma de Madrid, Madrid 28049, Spain
[2]Department of Materials Science and Engineering, Pennsylvania State University, University Park, Pennsylvania 16802, USA
[3]Advanced Technology Institute, Department of Electrical and Electronic Engineering, University of Surrey, Guildford GU2 7XH, United Kingdom
[4]Department of Chemistry and Biochemistry, University of Bern, Freiestrasse 3, 3012 Bern, Switzerland
[5]Institute of Low Temperature and Structure Research, Polish Academy of Science, Wroclaw, Poland
[6]Center for Nanoscale Materials, Argonne National Laboratory, Argonne, Illinois 60439, USA
[7]Instituto de Ciencia de Materiales de Madrid, ICMM, (CSIC), C/Sor Juana Inés de la Cruz 3, Madrid 28049, Spain
[8]Materials Theory, ETH Zurich, Wolfgang-Pauli-Strasse 27, 8093 Zürich, Switzerland

[a]**Authors to whom correspondence should be addressed:** mariola.ramirez@uam.es and vxg8@psu.edu
[b]This research was performed while I. Carrasco was at Dept. de Física de Materiales, Universidad Autónoma de Madrid, 28049 Madrid, Spain.
[c]This research was performed while U. Aschauer was at Materials Theory, ETH Zurich, Wolfgang-Pauli-Strasse 27, 8093 Zürich, Switzerland.

ABSTRACT

Polar instabilities are well known to be suppressed on scaling materials down to the nanoscale, when the electrostatic energy increase at surfaces exceeds lowering of the bulk polarization energy. Surprisingly, here we report an emergent low symmetry polar phase arising in nanoscale powders of $CaTiO_3$, the original mineral named perovskite discovered in 1839 and considered nominally nonpolar at any finite temperature in the bulk. Using nonlinear optics and spectroscopy, X-ray diffraction, and microscopy studies, we discover a well-defined polar to non-polar transition at a T_C = 350 K in these powders. The same polar phase is also seen as a surface layer in bulk $CaTiO_3$ single crystals, forming striking domains with in-plane polarization orientations. Density functional theory reveals that oxygen octahedral distortions in the surface layer lead to the stabilization of the observed monoclinic polar phase. These results reveal new ways of overcoming the scaling limits to polarization in perovskites.

Ferroelectricity can be unlocked in nominally non-polar materials such as $CaTiO_3$ and $SrTiO_3$ via different strategies such as chemical doping,[1–5] epitaxial strain,[6–10] and domain engineering.[11–16] For example, doped $Sr_{1-x}Ca_xTiO_3$ ceramics[3] and single crystals[4,5] show low temperature ferroelectric transitions of T_C < 40 K, with ferroelectricity arising from chemical strains imposed by different sized Sr^{2+} and Ca^{2+} ions in the structure. When grown as thin films, epitaxial strain can also drive $CaTiO_3$[8,10] and $SrTiO_3$[6,9] to become ferroelectric, as theory suggests;[10,17,18] however, ferroelectricity in stoichiometric thin films disappears below 5-10 nm in thickness.[19–21] Non-stoichiometric defects can stabilize ferroelectricity, as

has been shown in $SrTiO_3$ thin films.[22] Interestingly, these defect dipoles can align when scaled to smaller dimensions giving rise to ferroelectricity in a few nanometer thick $SrTiO_3$ films,[23] an example of a reverse thickness scaling effect. Similarly, ferroelectricity has been observed confined to ferroelastic domain boundaries in single crystal $CaTiO_3$,[13,14] arising from an improper ferroelectric mechanism.[24,25] Domain walls in ferroelectrics are typically on the order of a few unit cells in thickness,[26–28] which is the smallest possible scale on which ferroelectrics can be manipulated.[29]

With this background, we pose the following question: can room temperature polarization be unlocked in such paraelectric materials in powder and single crystal form, rather than as thin films? Furthermore, can it be achieved without intentionally doping, inducing non-stoichiometry, or external straining? Here, using complementary optical probe techniques including second harmonic generation (SHG), Raman spectroscopy, photoluminescence, and X-ray spectroscopy, we demonstrate that a low symmetry polar phase is stabilized in $CaTiO_3$ nanoparticles with a T_c above room temperature (350 K). Strikingly, this phase is also discovered as a surface layer in bulk single crystals of $CaTiO_3$. Density Functional Theory (DFT) reveals the origin of this phase as octahedral distortions that lead to reduced symmetry from orthorhombic (*mmm*) in bulk to monoclinic (*m*) in a surface layer with dominantly in-plane polarization. This emergent phase does not require any extrinsic defects such as doping, non-stoichiometry, or epitaxial strain. It is an exciting discovery for a mineral discovered 179 years ago and originally named *Perovskite*, a name that is synonymous today with a huge family of ABO_3 octahedral compounds.

To study the polar behavior of $CaTiO_3$, nanoparticles and bulk single crystal samples were prepared for measurements as discussed in the Supplementary Material. Figure 1(a) shows a scanning electron microscope (SEM) image of $CaTiO_3$ nanoparticles (NPs) with an average diameter of 40 nm. To study the polar response of these samples, we employed optical second harmonic generation, where two photons of light at frequency ω are converted into one photon of light at frequency 2ω. Electric dipole quadratic SHG occurs only in a nonlinear material which has broken inversion symmetry, a necessary condition for a polar phase.[30–32] Figure 1(b) shows the SHG intensity ($I^{2\omega}$) measured from the 40 nm $CaTiO_3$ NPs during heating and cooling scans (see experimental section for details). The SHG intensity decreases sharply around 350 K, indicating a transition from a low-temperature polar phase (SHG active) to a high-temperature non-polar phase (SHG inactive). Hysteresis is also observed in the SHG intensity upon heating and cooling, which is commonly observed during ferroelectric phase transitions.[33]

An additional test was performed by measuring the temperature evolution of the Raman spectra of the $CaTiO_3$ NPs shown in Fig. 1(c). Raman spectroscopy is a powerful tool that probes the lattice dynamics in a material, yielding important information about the structure and phase transitions[34] and has been successfully applied to many bulk ferroelectric perovskite systems such as $BaTiO_3$ and $PbTiO_3$.[35–40] Upon

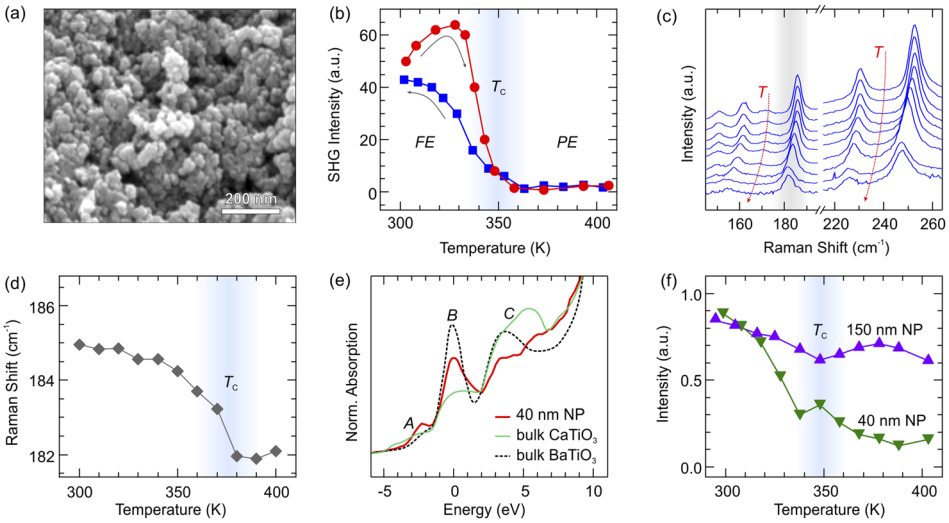

FIG. 1. (a) SEM image of $CaTiO_3$ NPs with an average size of 40 nm. (b) Temperature dependence of the SHG intensity from the $CaTiO_3$ NP sample with arrows indicating the direction of temperature with red circles for heating and blue squares for cooling scans. The phase transition temperature is approximately T_C = 350 K as shown by the highlighted blue region. (c) Temperature dependent Raman spectra (150-450 K) of the $CaTiO_3$ NPs. The spectra were vertically shifted for sake of comparison. (d) Raman shift of the 185 cm^{-1} active Raman mode as a function of temperature. The highlighted blue region denotes T_C. (e) Detailed view of the pre-edge fine structure peaks of the Ti K-edge XANES spectrum obtained at 40 K from 40 nm $CaTiO_3$ NPs (red line) compared with bulk $CaTiO_3$ (solid green line) and $BaTiO_3$ (dashed black line) from Vedrinskii *et al.*[42] The A, B, and C peaks are shown, with A being from t_{2g} and B and C being from e_g crystals orbitals of the Ti atom. (f) Temperature dependence of integrated emission intensity corresponding to the $^4F_{3/2} \rightarrow {}^4I_{11/2}$ electronic transition of Nd^{3+} in $CaTiO_3$ samples with an average NP size of 40 nm (green down-pointing triangles) and 150 nm (blue up-pointing triangles). The blue shadow area indicates the ferroelectric phase transition.

heating, the Raman modes of the $CaTiO_3$ NPs shift to lower frequency, which is typical of a ferroelectric-to-paraelectric phase transition. The shift in the center of mass of the 185 cm^{-1} Raman mode with temperature is plotted in Fig. 1(d), revealing a ferroelectric transition temperature of approximately $T_C \sim 350$-370 K, which agrees very well with temperature dependent SHG measurements.

The polarization of the $CaTiO_3$ NPs is further supported by X-ray absorption near edge structure (XANES) analysis (see Supplementary Material for experimental details). This technique directly probes the anisotropy of TiO_6 oxygen octahedra in $ATiO_3$ perovskites (A = Pb, Ba, Sr, Ca, Eu),[41,42] where strong qualitative differences are observed between ferroelectric and paraelectric materials in their pre-edge fine structure of the X-ray Ti K-absorption spectra. The pre-edge features in Ti-based perovskites are composed of three main peaks (A, B, C), which are caused by transitions of the Ti 3s electron to unoccupied electron states near the bottom of the conduction band formed by empty 3*d* orbitals. Of the three peaks, the B peak is commonly considered to be a strong qualitative indicator of ferroelectricity; it is mainly caused by the *p*-*d* mixture effect and, since its magnitude depends on the TiO_6 tetragonal deformation, it can be used to determine the mean-square displacements of Ti atoms from their octahedral centers.[42] As shown in Fig. 1(e), the intensity of the B peak is much more pronounced for ferroelectric crystals such as bulk $BaTiO_3$ where Ti is displaced from the center of the TiO_6 cage, and the B peak is much weaker for paraelectric crystals such as $CaTiO_3$ where Ti is centered in the TiO_6 cage. In comparison, the XANES spectra obtained for the 40 nm $CaTiO_3$ NPs show a much more intense B peak as compared to bulk and approach that of bulk $BaTiO_3$.

To evaluate the role of the nanoparticle size on the polar behavior in $CaTiO_3$, we used temperature dependent rare-earth based photoluminescence analysis on both 40 nm and 150 nm average NP size samples (see the supplementary material for experimental details). Photoluminescence (PL) from rare-earth ions is a sensitive tool to analyze symmetry breaking from a low-temperature ferroelectric phase (more PL active) to a high-temperature paraelectric phase (less PL active).[43-46] In particular, the *f*-*f* optical transitions of Nd^{3+} ion dopants can act as a sort of structural probe. The spontaneous emission of Nd^{3+} ions in $CaTiO_3$ samples is comprised of both bulk and surface contributions, and the spectroscopic phase-transition signatures are sensitive to the surface-to-volume ratio, as demonstrated in Fig. 1(f). For both 40 nm and 150 nm NP sizes, a phase transition is observed around 350 K, indicated by the abrupt intensity change in the emission area of the $^4F_{3/2} \rightarrow {}^4I_{11/2}$ optical transition of Nd^{3+} ions in the samples. Assuming that the majority of background signal is coming from the non-polar phase, the relative change in intensity across the transition indicates that the polar contribution of the 40 nm NPs to the overall photoluminescence spectrum is 80% while the contribution from the 150 nm-sized NPs, which have a lower surface to volume ratio, is close to 40%. This is a strong indication that $CaTiO_3$ NPs behave differently with respect to bulk and suggests a significant thickness for the polar surface layer (estimated to be *at least* ~ 10-20 nm thick).

To gain microscopic insight into this unusual phase transition and to spatially isolate the role of the twin walls versus the surface layer effects, we performed polarized confocal spectroscopic Raman and SHG imaging at the $(110)_0$ surface of a $CaTiO_3$ single crystal (see the supplementary material for sample preparation details). Raman modes strongly depend on the input ($E^{\omega 0}$) and output ($E^{\omega 0-\Delta\omega}$) polarization states of light, and the intensity variations of different Raman modes can be exploited in a variety of ways to spectroscopically visualize the twin domain structure of $CaTiO_3$, which is composed of $(112)_0$ and $(110)_0$ ferroelastic domains rotated by 90° and 180°, respectively.[47] The Raman intensity distribution maps in Fig. 2(a) were constructed by measuring Raman peaks shown in Fig. 2(b) that centered around 230 cm^{-1} and 485 cm^{-1}. The Raman spectra of the $CaTiO_3$ single crystal are shown in comparison with the spectra for the 40 nm NP sample, which shows all of the active Raman modes, since the NPs do not have any specific orientation. Depending on the input/output polarization of light, different regions of the crystal surface light up, revealing a zigzag domain structure that is related to the underlying twin domains in the $CaTiO_3$ crystal. There are four main domains (labeled 1-4) and these are split into two main groups, whose in-plane crystal axes are rotated by 90° with respect to the other. A schematic of the domain structure is shown in Fig. 2(c), with the orientation of the lab axes (*x*, *y*, *z*) shown with respect to the orthorhombic *Pbnm* axes (*a*, *b*, *c*).

Having established the twin structure, polarization dependent spatially resolved SHG microscopy scans were performed at the same region, showing the four major types of polar domains with orthogonal polarization directions, displayed in Fig. 2(d). The SHG microscopy images directly map to the Raman intensity maps, establishing that there is indeed a reduction in the symmetry at the surface of the crystal. The four domains show pronounced polarization dependence of the input electric field of light (E^{ω}) and direction of the measured second harmonic electric field ($E^{2\omega}$). The presence of a significant SHG signal in all of the uniform domains indicates a common absence of structural inversion symmetry and a deviation from the non-polar bulk *Pbnm* structure of $CaTiO_3$. To further probe their local symmetry, we performed SHG polarimetry, which yields accurate information on the local point group symmetry of a material. Figure 2(e) shows the measured SHG intensity ($I^{2\omega}$) as the fundamental field is rotated by $\phi = 360°$ around the *z* axis. The experimental SHG data shown in Fig. 2(e) can only be modeled using a monoclinic mirror plane (*m*), indicating that the surface symmetry of $CaTiO_3$ surface reduces from bulk *mmm* to *m* point group symmetry with the mirror plane perpendicular to the *c* axis, allowing for polarization in the *ab* plane.

To gain more information about the local structure at the $CaTiO_3$ surface, we performed nanoscale Scanning X-ray Diffraction Microscopy (nano-SXDM)[15,16,48,49] on the same sample area, as shown in Fig. 3(a). The nano-SXDM experiments monitored the different $(220)_0$ diffraction peaks of the

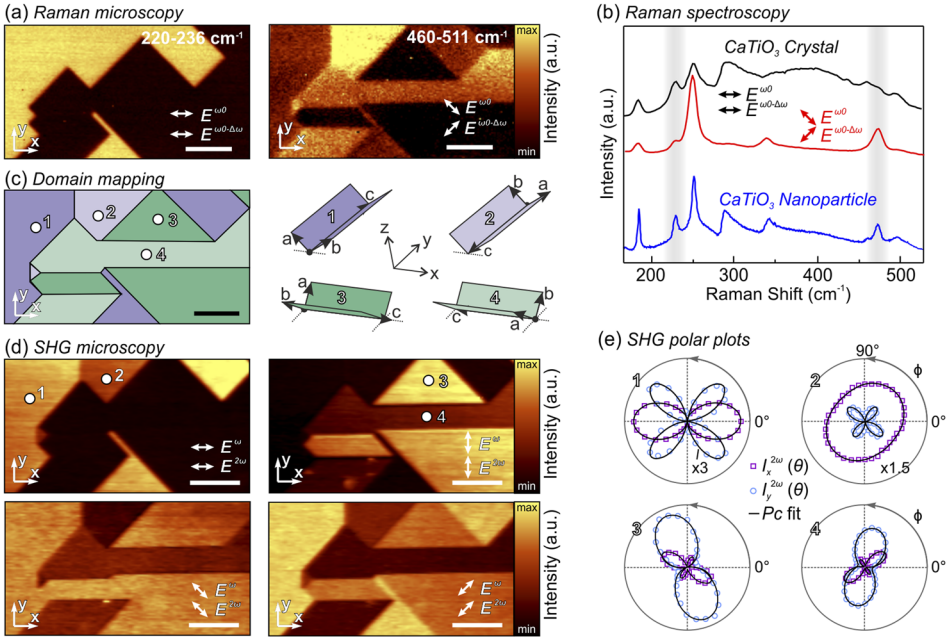

FIG. 2. (a) Raman mapping of a $(110)_0$ $CaTiO_3$ bulk single crystal surface, with the white bar being 8 μm. The direction of the fundamental input light ($E^{\omega 0}$) and generated output light ($E^{\omega 0-\Delta\omega}$) are shown together with the *x*-*y* lab axes on the bottom left. (b) Raman spectroscopy of the $CaTiO_3$ single crystal with vertical (red) and horizontal (black) input/output configurations on the top. For comparison, the spectra for $CaTiO_3$ NPs (blue) are shown at the bottom. (c) Schematic of the domain structure at the surface of the single crystal sample. The different domain variants are shown on the right along with the *a*, *b*, and *c* orthorhombic axes. (d) SHG microscopy images of the same region shown in (a). The polarization directions of the fundamental (E^{ω}) and second harmonic ($E^{2\omega}$) are shown on the bottom right, with the white bar being 8 μm. (e) SHG polar plots for the locations 1-4 shown in (d), with SHG intensity along *x* and *y* ($I_x^{2\omega}$ and $I_y^{2\omega}$) shown as purple squares and blue circles, respectively. Theory fits to the data using a monoclinic *Pc* model shown as black lines. The angle ϕ is the degree between E^{ω} and the *x* axis.

four different domain variants. The crystallographic domain types each have a slightly different orientation and thus diffraction condition of their $(220)_0$ reflection which can be spatially resolved. The observed domain structure is in excellent agreement with that obtained from Raman and SHG domain imaging.

Nano-SXDM is extremely sensitive to local deviations from the bulk structure, and such structural distortions will appear as additional diffraction peaks near the nominal bulk diffraction condition. Within the $CaTiO_3$ domain structure, such additional diffraction intensity is ubiquitous, as is illustrated by the representative diffraction images from each of the four domain types in Fig. 3(b). Throughout the entire domain structure, weaker diffraction peaks are observed in addition to the nominal $(220)_0$ bulk reflection, which are labeled as bulk and surface. We ascribe these diffraction signatures to a distorted (polar) monoclinic structure present near the $CaTiO_3$ surface. The observed nano-SXDM features correspond to the distorted minority phase present within the first several microns (probing depth of the X-rays) of the sample

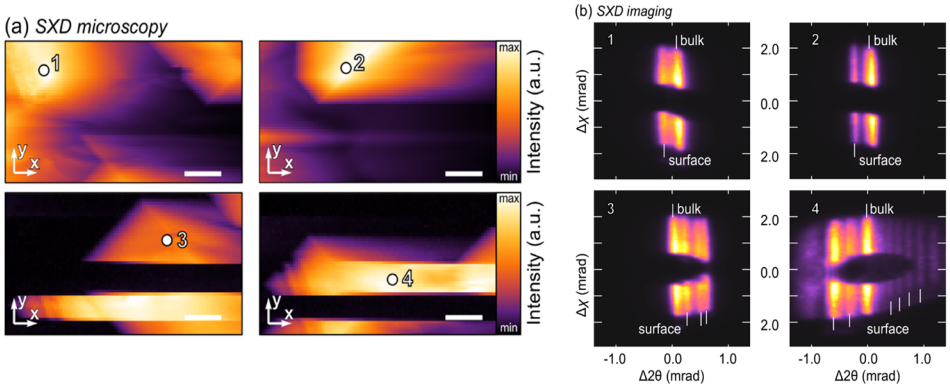

FIG. 3. (a) SXDM microscopy of the same crystal region shown in Fig. 2, displaying the integrated intensity of the diffraction peak corresponding to domains 1 through 4. (b) Background-subtracted 2D diffraction images recorded at the positions shown in (a). The positions of the nominal bulk and anomalous surface diffraction are indicated by white lines.

surface and therefore necessarily correspond to the surface polar structure observed in the SHG experiments.

After having experimentally shown that a polar phase is locally confined to a surface layer of $CaTiO_3$ well above room temperature, we used density functional theory (DFT) to obtain a complete picture of the $CaTiO_3$ surface structure. To compare with the above single-crystal experiments, we chose the same surface orientation, but note that for a nanoparticle, (110) surfaces of different orientations may be present. Figure 4(a) displays a relaxed structure for several layers of $CaTiO_3$, with the central unit cell layer having frozen-in bulk structure parameters of $CaTiO_3$. The surface coordinates (x, y, z) and the orthorhombic *Pbnm* axes (a, b, c) are shown next to the atomic structure. Layer-resolved polarization values were calculated from the atomic structure and are plotted in Fig. 4(b). In the frozen layer, the polarization is zero in all directions as expected for bulk $CaTiO_3$. In the relaxed layers, an in-plane polarization emerges along the y direction (P_y), which oscillates between approximately P_y = 0.4 $\mu C/cm^2$ in the CaO layers and P_y = 0.8 $\mu C/cm^2$ in the TiO_2 layers. The out-of-plane polarization (P_z) at the surface is a result of the inward relaxation of the outermost layers. No polarization is seen along the x direction (P_x), which is in excellent agreement with the monoclinic mirror plane symmetry of the polar phase determined by SHG polarimetry analysis. Figure 4(c) shows the layer-averaged displacements along the in-plane directions (Δx, Δy), which are nearly zero in the frozen layer and within the adjacent relaxed layers. Displacements along the y direction are seen, with larger average displacements in the TiO_2 layers ($\Delta y \sim 6$ pm) compared to the CaO layer ($\Delta y \sim 3$ pm). The layer-averaged rotation angle changes are plotted in Fig. 4(d), revealing that only the rotations around the x axis ($\Delta\alpha$) are changed, resulting in ionic displacements along the y and z directions. The averaging over layers puts in evidence that the unbalanced octahedral rotations are due to the presence of the surface, as the rotations would be perfectly balanced when averaging over the layers in bulk. The DFT calculations suggest that an unbalanced unwinding of the octahedral rotations around the x axis results in ionic displacements along the y direction, proportional to the angle changes and additive for the layers as one moves from the bulk frozen layer toward the relaxed surface layers. The net displacements in the y direction in each layer lead to the emergence of the polarization along the y direction, while it is absent along the perpendicular x direction where no unbalanced octahedral rotations are present. Based on these findings, a potential explanation for the above-mentioned phase transition at 350 K is that thermal vibrations undo the atomic displacements leading to polarization.

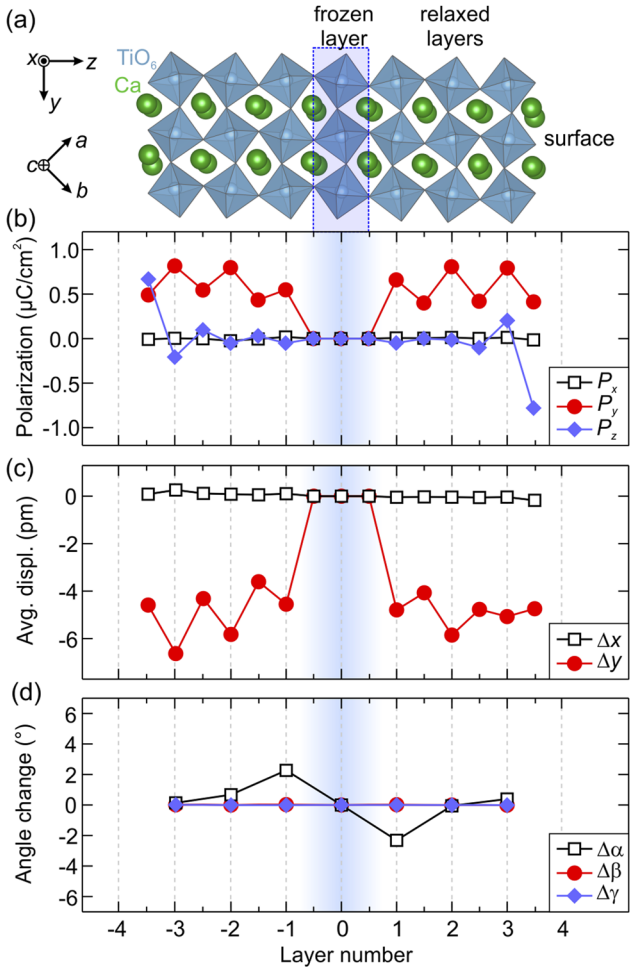

FIG. 4. (a) Structural model of $CaTiO_3$ with the middle section frozen to the bulk lattice parameter values and the structure relaxed along the z direction. The lab axes are shown above, and the orthorhombic lattice parameter orientation are shown below. The Ca atoms are green, and the TiO_6 octahedra are blue. (b) Layer-resolved polarization computed using nominal ionic charges. (c) Layer-averaged displacements along the in-plane directions, and (d) angle changes, with the center of the frozen layer being 0.

Our results reveal an emergent polar monoclinic phase arising from a surface layer polar reconstruction involving oxygen octahedral distortions, providing a route to induce polar order in bulk quantum paraelectric powders and crystal surface layers. This *naturally* occurring layer is at least 10's of nanometers thick (approximately on the order of the particle size probed where this polar layer dominates bulk response) and perhaps up to several micrometers thick (upper limit set by the probing depth of X-rays). Furthermore, these layers are naturally epitaxial to the bulk of the particles or the crystals on which they form, thus providing an alternative to the epitaxial thin film growth route. Moreover, as the distortion of the octahedral units is intimately related to the stability of the perovskite phase, stabilizing a wide range of other emergent properties in the surface layer, including multiferroicity and metal-insulator transitions, could be envisaged.

See supplementary material for a detailed experimental description.

T.T.A.L., E.B., H.A., A.S.B., R.C.H., and V.G. gratefully acknowledge support from the National Science Foundation

Penn State MRSEC Center for Nanoscale Science Grant Nos. DMR-1420620 and DMR-1807768. V.G. acknowledges support from the Department of Energy Grant No. DE-SC0012375 for the X-ray diffraction microscopy work with Argonne National Laboratory. We gratefully thank Dr. A. N. Morozovska, Dr. E. A. Eliseev, and Professor J. M. Rondinelli for extensive theory discussions. M.O.R., C.H., P.M., and L.E.B. acknowledges funding from the Spanish Ministry of Economy and Competitiveness (MINECO) under Project No. MAT2016-76106-R and the Comunidad de Madrid Grant No. S2013/MIT-2740. L.E.B. and M.O.R. also acknowledges financial support from the Spanish Ministry of Economy and Competitiveness, through The "María de Maeztu" Programme for Units of Excellence in R&D (Grant No. MDM-2014-0377). U.A. and N.A.S. were financially supported by the ETH Zürich and by the ERC Advanced Grant program, No. 291151. Computer resources were provided by the ETH Zürich (Euler cluster). Assistance from SAMBA beamline staff at SOLEIL is acknowledged.

REFERENCES

[1] A. Chandra, R. Ranjan, D. Singh, N. Khare, and D. Pandey, J. Phys.: Condens. Matter **18**, 2977 (2006).
[2] D. Rytz, U. Höchli, and H. Bilz, Phys. Rev. B **22**, 359 (1980).
[3] T. Mitsui and W. B. Westphal, Phys. Rev. **124**, 1354 (1961).
[4] J. Bednorz and K. Müller, Phys. Rev. Lett. **52**, 2289 (1984).
[5] C. W. Rischau, X. Lin, C. P. Grams, D. Finck, S. Harms, J. Engelmayer, T. Lorenz, Y. Gallais, B. Fauqué, and J. Hemberger, Nat. Phys. **13**, 643 (2017).
[6] J. Haeni, P. Irvin, W. Chang, R. Uecker, P. Reiche, Y. Li, S. Choudhury, W. Tian, M. Hawley, and B. Craigo, Nature **430**, 758 (2004).
[7] D. G. Schlom, L.-Q. Chen, C.-B. Eom, K. M. Rabe, S. K. Streiffer, and J.-M. Triscone, Annu. Rev. Mater. Res. **37**, 589 (2007).
[8] R. C. Haislmaier, E. D. Grimley, M. D. Biegalski, J. M. LeBeau, S. Trolier-McKinstry, V. Gopalan, and R. Engel-Herbert, Adv. Funct. Mater. **26**, 7271 (2016).
[9] R. C. Haislmaier, R. Engel-Herbert, and V. Gopalan, Appl. Phys. Lett. **109**, 032901 (2016).
[10] M. D. Biegalski, L. Qiao, Y. Gu, A. Mehta, Q. He, Y. Takamura, A. Borisevich, and L.-Q. Chen, Appl. Phys. Lett. **106**, 162904 (2015).
[11] J. Scott, E. Salje, and M. Carpenter, Phys. Rev. Lett. **109**, 187601 (2012).
[12] E. Salje and H. Zhang, Phase Transitions **82**, 452 (2009).
[13] S. Van Aert, S. Turner, R. Delville, D. Schryvers, G. Van Tendeloo, and E. K. Salje, Adv. Mater. **24**, 523 (2012).
[14] L. Goncalves-Ferreira, S. A. Redfern, E. Artacho, and E. K. Salje, Phys. Rev. Lett. **101**, 097602 (2008).
[15] T. T. Lummen, Y. Gu, J. Wang, S. Lei, F. Xue, A. Kumar, A. T. Barnes, E. Barnes, S. Denev, and A. Belianinov, Nat. Commun. **5**, 3172 (2014).
[16] T. T. Lummen, J. Leung, A. Kumar, X. Wu, Y. Ren, B. K. VanLeeuwen, R. C. Haislmaier, M. Holt, K. Lai, and S. V. Kalinin, Adv. Mater. **29**, 1700530 (2017).
[17] Y. Gu, K. Rabe, E. Bousquet, V. Gopalan, and L.-Q. Chen, Phys. Rev. B **85**, 064117 (2012).
[18] C.-J. Eklund, C. Fennie, and K. Rabe, Phys. Rev. B **79**, 220101 (2009).
[19] D. A. Tenne, P. Turner, J. Schmidt, M. Biegalski, Y. Li, L. Chen, A. Soukiassian, S. Trolier-McKinstry, D. Schlom, and X. Xi, Phys. Rev. Lett. **103**, 177601 (2009).
[20] J. F. Ihlefeld, D. T. Harris, R. Keech, J. L. Jones, J. P. Maria, and S. Trolier-McKinstry, J. Am. Ceram. Soc. **99**, 2537 (2016).
[21] D. D. Fong, G. B. Stephenson, S. K. Streiffer, J. A. Eastman, O. Auciello, P. H. Fuoss, and C. Thompson, Science **304**, 1650 (2004).
[22] H. Jang, A. Kumar, S. Denev, M. D. Biegalski, P. Maksymovych, C. Bark, C. T. Nelson, C. Folkman, S. H. Baek, and N. Balke, Phys. Rev. Lett. **104**, 197601 (2010).
[23] D. Lee, H. Lu, Y. Gu, S.-Y. Choi, S.-D. Li, S. Ryu, T. Paudel, K. Song, E. Mikheev, and S. Lee, Science **349**, 1314 (2015).
[24] P. Barone, D. Di Sante, and S. Picozzi, Phys. Rev. B **89**, 144104 (2014).
[25] A. N. Morozovska, E. A. Eliseev, M. D. Glinchuk, L.-Q. Chen, and V. Gopalan, Phys. Rev. B **85**, 094107 (2012).
[26] C. Kittel, Solid State Commun. **10**, 119 (1972).
[27] B. Meyer and D. Vanderbilt, Phys. Rev. B **65**, 104111 (2002).
[28] A. K. Tagantsev, L. E. Cross, and J. Fousek, *Domains in Ferroic Crystals and Thin Films* (Springer, 2010).
[29] G. Catalan, J. Seidel, R. Ramesh, and J. F. Scott, Rev. Modern. Phys. **84**, 119 (2012).
[30] S. A. Denev, T. T. Lummen, E. Barnes, A. Kumar, and V. Gopalan, J. Am. Ceram. Soc. **94**, 2699 (2011).
[31] R. W. Boyd, *Nonlinear Optics* (Academic press, 2003).
[32] J. Nordlander, G. De Luca, N. Strkalj, M. Fiebig, and M. Trassin, Appl. Sci. **8**, 570 (2018).
[33] L. M. Garten, M. Burch, A. S. Gupta, R. Haislmaier, V. Gopalan, E. C. Dickey, and S. Trolier-McKinstry, J. Am. Ceram. Soc. **99**, 1645 (2016).
[34] D. A. Tenne and X. Xi, J. Am. Ceram. Soc. **91**, 1820 (2008).
[35] C. Perry and D. Hall, Phys. Rev. Lett. **15**, 700 (1965).
[36] A. Scalabrin, A. Chaves, D. Shim, and S. Porto, Phys. Status Solidi B **79**, 731 (1977).
[37] M. DiDomenico, Jr., S. Wemple, S. Porto, and R. Bauman, Phys. Rev. **174**, 522 (1968).
[38] G. Burns and F. Dacol, Phys. Rev. B **18**, 5750 (1978).
[39] G. Burns and B. A. Scott, Phys. Rev. Lett. **25**, 167 (1970).
[40] G. Burns and B. A. Scott, Phys. Rev. B **7**, 3088 (1973).
[41] B. Ravel and E. Stern, Physica B **208**, 316–318 (1995).
[42] R. Vedrinskii, V. Kraizman, A. Novakovich, P. V. Demekhin, and S. Urazhdin, J. Phys.: Condens. Matter **10**, 9561 (1998).
[43] K. R. Kandula, S. S. K. Raavi, and S. Asthana, J. Alloys Compd. **732**, 233 (2018).
[44] P. Zhang, M. Shen, L. Fang, F. Zheng, X. Wu, J. Shen, and H. Chen, Appl. Phys. Lett. **92**, 222908 (2008).
[45] M. O Ramirez, L. E Bausá, A. Speghini, M. Bettinelli, L. Ivleva, and J. G. Solé, Phys. Rev. B **73**, 035119 (2006).
[46] M. O Ramírez, D. Jaque, L. E Bausá, J. G. Solé, and A. Kaminskii, Phys. Rev. Lett. **95**, 267401 (2005).
[47] H. Kay and P. Bailey, Acta Crystallogr. **10**, 219 (1957).
[48] A. Ying, B. Osting, I. Noyan, C. E. Murray, M. Holt, and J. Maser, J. Appl. Crystallogr. **43**, 587 (2010).
[49] M. Holt, R. Harder, R. Winarski, and V. Rose, Annu. Rev. Mater. Res. **43**, 183 (2013).